Elsevier Editorial System(tm) for Chemical Engineering Journal

Manuscript Draft

Manuscript Number:

Title: The investigation of blue shift, crystal field theory and photoionization effect in Mn4+-doped La2-xYxMgTiO6 red phosphor for plant growth LED lighting

Article Type: Research Paper

Section/Category: Novel Materials for Energy and Advanced Applications

Keywords: La2-xYxMgTiO6:Mn4+; Cation substitution; Tunable photoluminescence; Thermal stability; Plant growth LED lighting.

Corresponding Author: Professor Zhi Zhou, Ph.D

Corresponding Author's Institution: Hunan Agricultural University

First Author: Shujie Gai

Order of Authors: Shujie Gai; Haifeng Zhu; Yuan Zhong; Peixing Gao; Cheng Zhou; Zihui Kong; Maxim S. Molokeev; Mao Xia; Zhi Zhou, Ph.D

Abstract: Currently, phosphor-converted LED (pc-LEDs) are revolutionizing the industry of plant growth lighting. To meet the requirements of this technology, phosphors with tunable photoluminescence, high thermal stability and quantum efficiency are required. Herein, we found that the simple substitution of yttrium for lanthanum in La2MgTiO6:Mn4+ system could satisfy above three criteria simultaneously. The photoluminescence properties can be regulated by continuously controlling the chemical composition of La2-xYxMgTiO6:Mn4+ solid solution. The La sites are occupied by Y ions, causing a significant blue shift in the emission spectra which owing to the change of local crystal field strengthen. Meanwhile, the thermal stability and decay lifetimes are also varied due to the variation of band gap energy. Besides, luminous intensity, thermal stability and internal quantum efficiency (IQE) increased by 201.8%, 26%, and 23%, respectively. The electronic luminescence (EL) of pc-LED devices using La2-xYxMgTiO6:Mn4+ red phosphor is evaluated, which matching the absorption regions of plant pigments well, reflecting the superiority of the studied phosphors in plant growth lighting areas.

Suggested Reviewers: Guogang Li
Faculty of Materials Science and Chemistry, China University of Geosciences
ggli@cug.edu.cn
Prof. Li is good at the investigations about luminescent materials.

Ru-Shi Liu
Department of Chemistry, National Taiwan University
rsliu@ntu.edu.tw
We believe the comments from Prof. Liu would be relevant and useful because he is an expert in this field.

Yongfu Liu

Ningbo Institute of Materials Technology and Engineering, Chinese Academy of Sciences
liuyongfu@nimte.ac.cn
An activate and respective researcher in the field of inorganic luminescent materials.

Opposed Reviewers:

Dear editor,

We would like to submit this paper, "**The investigation of blue shift, crystal field theory and photoionization effect in $Mn^{4+}$-doped $La_{2-x}Y_xMgTiO_6$ red phosphor for plant growth LED lighting**", to *Chemical Engineering Journal* which is one of the impactful journals in materials science. The submission of this manuscript has been approved by the authors and has been submitted exclusively to *Chemical Engineering Journal*. The work reported therein has not been published, or submitted for publication, elsewhere in any medium of a public nature, including electronic journals and computer databases.

Phosphor is an essential component in phosphor-converted light-emitting-diodes (pc-LEDs). As for indoor plant cultivation, a certain amount of far red light could improve the quality and yields of crops. Therefore, it is urgent to discover a high-efficient and far-red-emitting phosphor for indoor plant cultivation. In this work, we designed and prepared the new double perovskite type solid solution phosphors of $La_{2-x}Y_xMgTiO_6$:0.002$Mn^{4+}$ with controllable photoluminescence properties. It would distort the crystal structure of $La_2MgTiO_6$ and the characteristic diffraction peaks shifted toward higher 2θ angle, which originated from the shrinkage of the crystal cell. The impacts of this modulations on the photoluminescence properties of $La_2MgTiO_6$:$Mn^{4+}$ could be divided into following aspects:

- **201.8% and 26%** enhancements of the emission intensity and thermal stability was observed.
- Doping $Y^{3+}$ could also induce an obvious **blue shift** of $La_2MgTiO_6$:$Mn^{4+}$ from 710.8 nm to 699.8 nm (11 nm).
- The IQE and EQE of $La_2MgTiO_6$:$Mn^{4+}$ was enhanced from 32.5% and 22.2% to **55.5%** and **42.5%** after $Y^{3+}$ doped.

In order to comprehensively understand the origin of these enhancements, a great amount of measurements and theoretical investigations, including powder XRD Rietveld refinement, UV-vis absorption spectra, PLE & PL, crystal field strength, Tanabe−Sugano energy level diagram, and decay times were conducted. The **thermal stabilities** and **decay lifetimes** of these phosphors were investigated as well and the local structures diagram was employed to interpretate it theoretically. Finally, the excellent electronic luminescence properties and unique emission in blue and far red

region of as-fabricated LED devices demonstrates that these phosphors have promising application in plant growth LED lighting.

We believe this paper is suitable for ***Chemical Engineering Journal***.

Thank you for your consideration, and we are looking forward to receiving positive comments from the reviewers. If you have any queries, please don't hesitate to contact me at the address below.

Best regards!

Yours Sincerely,

Corresponding author:
Prof. Zhi Zhou
Hunan Optical Agriculture Engineering Technology Research Center
College of Science
Hunan Agricultural University
Changsha 410128, P. R. China
E-mail: zhouzhi@hunau.edu.cn

# List of Suggested Reviewers

**Guogang Li**
Engineering Research Center of Nano-Geomaterials of Ministry of Education, Faculty of Materials Science and Chemistry, China University of Geosciences, Wuhan 430074, P. R. China
E-mail: ggli@cug.edu.cn
Reason: Prof. Li is good at the investigations about luminescent materials.

**Ru-Shi Liu**
Department of Chemistry, National Taiwan University, Taipei 106, Taiwan
E-mail: rsliu@ntu.edu.tw
Reason: We believe the comments from Prof. Liu would be relevant and useful because he is an expert in this field.

**Yongfu Liu**
Ningbo Institute of Materials Technology and Engineering, Chinese Academy of Sciences, Ningbo, 315201, PR China
E-mail: liuyongfu@nimte.ac.cn
Reason: An activate and respective researcher in the field of inorganic luminescent materials.

## Graphical Abstract

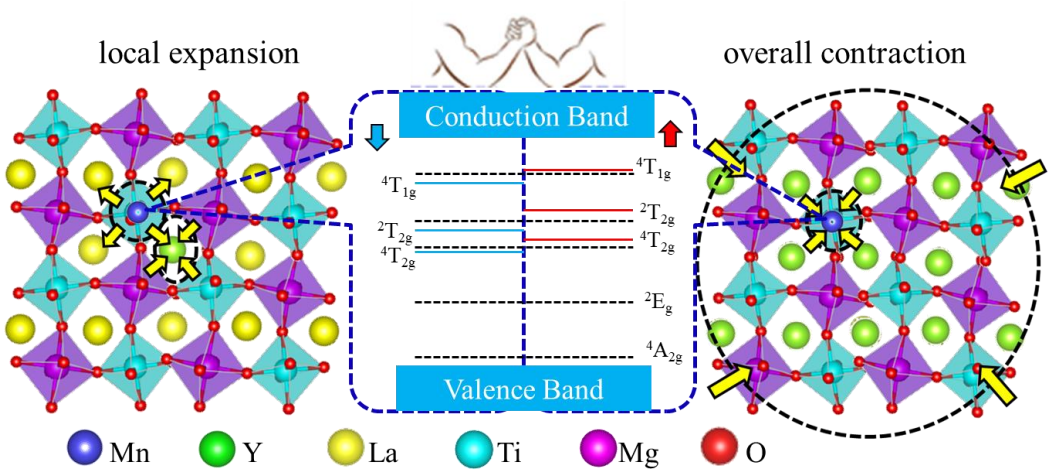

# Highlights

1. The luminescent intensity, thermal stability and QE are improved by adding Y ions.
2. The mechanism of tunable luminescent, changes of thermal stability are discussed.
3. The emission region of pc-LEDs matched well with the absorption of plant pigments.

# The investigation of blue shift, crystal field theory and photoionization effect in $Mn^{4+}$-doped $La_{2-x}Y_xMgTiO_6$ red phosphor for plant growth LED lighting

Shujie Gai[a,b,1], Haifeng Zhu[a,b,1], Yuan Zhong[a,b], Peixing Gao[a], Cheng Zhou[a], Zihui Kong[a], Maxim S. Molokeev[c,d], Mao Xia[a,b]*, Zhi Zhou[a,b]*

[a]School of Chemistry and Materials Science, Hunan Agricultural University, Changsha, 410128, P.R. China

[b]Hunan Optical Agriculture Engineering Technology Research Center, Changsha, 410128, P. R. China

[c]Laboratory of Crystal Physics, Kirensky Institute of Physics, Federal Research Center KSC SB RAS, Krasnoyarsk 660036, Russia

[d]Siberian Federal University, Krasnoyarsk, 660041, Russia

***Corresponding authors:**
Prof. Zhi Zhou
**Phone number:** (+86)-13975160917; **E-mail:** zhouzhi@hunau.edu.cn
Ph. D. Mao Xia
**Phone number:** (+86)-15802612087; **E-mail:** xiamao2019@hunau.edu.cn
[1] Shujie Gai and Haifeng Zhu contributed equally to this work.

**Abstract:**

Currently, phosphor-converted LED (pc-LEDs) are revolutionizing the industry of plant growth lighting. To meet the requirements of this technology, phosphors with tunable photoluminescence, high thermal stability and quantum efficiency are required. Herein, we found that the simple substitution of yttrium for lanthanum in $La_2MgTiO_6:Mn^{4+}$ system could satisfy above three criteria simultaneously. The photoluminescence properties can be regulated by continuously controlling the chemical composition of $La_{2-x}Y_xMgTiO_6:Mn^{4+}$ solid solution. The La sites are occupied by Y ions, causing a significant blue shift in the emission spectra which owing to the change of local crystal field strengthen. Meanwhile, the thermal stability and decay lifetimes are also varied due to the variation of band gap energy. Besides, luminous intensity, thermal stability and internal quantum efficiency (IQE) increased by 201.8%, 26%, and 23%, respectively. The electronic luminescence (EL) of pc-LED devices using $La_{2-x}Y_xMgTiO_6:Mn^{4+}$ red phosphor is evaluated, which matching the absorption regions of plant pigments well, reflecting the superiority of the studied phosphors in plant growth lighting areas.

**Keywords:** $La_{2-x}Y_xMgTiO_6:Mn^{4+}$; Cation substitution; Tunable photoluminescence; Thermal stability; Plant growth LED lighting.

## 1. Introduction

Facility agriculture, as an effective strategy to increase the added value of agricultural products, is used worldwide with the development of modern agriculture technology [1-3]. This is because it can provide adjustable growth parameters for

plant growth and development, and ensures the quality and yield of agricultural products [4,5]. Among them, supplemental light is a key technical parameter that can directly regulate plant growth and development, morphogenesis and physiological metabolism, etc., which helps it to improve the growth rate of crops, accelerate the accumulation of photosynthetic products and enhance the quality of agricultural products [6,7]. Researches show that the photosynthetic pigments (including chlorophyll A, chlorophyll B, and carotenoids) and phytochrome (including $P_R$ and $P_{FR}$) are mainly absorb blue (390-500 nm), red (590-690 nm), and far-red (690-800 nm) light, which participate in regulating the entire process of photosynthesis, germination, growth and flowering in plants [8,9]. At present, the LED plant growth lamp composed of "blue light chip + red phosphors" has replaced the conventional light source and has been widely used in facility agriculture [5,10,11]. Although the commercial red phosphor (such as $Ca_{1-x-y}Sr_xBa_yAlSiN_3:Eu^{2+}$, $Ca_{2-x-y}Sr_xBa_ySi_5N_8: Eu^{2+}$ and $K_2SiF_6:Mn^{4+}$ phosphor) have superior luminous properties, their raw materials are expensive and the far-red light component is rare in their emission spectra, which make them cannot meet the light requirements of plants and has greatly limited its application in the field of agricultural lighting [12-15]. Therefore, obtain a far-red phosphor with high luminous performance is an important and difficult problem in the research of plant supplement light.

As a tetravalent transition metal, manganese ($Mn^{4+}$) has a $3d^3$ electron configuration and usually exhibits red or far-red emission in fluorides and oxides[16,17]. For $Mn^{4+}$ activated phosphors, the luminescence performance is

closely related to the crystal field environment around the luminescence center. In general, $Mn^{4+}$ prefers to occupy the octahedral lattice sites and the luminescence properties can be adjusted by changing the arrangement, distortion and tilt of the octahedral lattice [18,19]. Up to date, matrix materials with dual perovskite structures (such as $La_2MgTiO_6$ [20], $Y_2MgTiO_6$ [21,22], $La_2CaHfO_6$ [23] and $La_2MgGeO_6$ [24], etc.) have the advantages of good chemical stability, thermal stability, easy preparation. The abundant population of [$TiO_6$], [$MgO_6$], [$HfO_6$] and [$GeO_6$] octahedral in these phosphors provide possible occupying sites for $Mn^{4+}$ ions. For $La_2MgTiO_6$:$Mn^{4+}$ (LMT:$Mn^{4+}$) phosphor, it can be excited efficiently by a blue LED chip and exhibit red and far-red emission with emission peak at about 710 nm, showed a promising usage as plant-growth-lighting materials [20]. However, to further realize the application of this phosphor in plant growth lighting, the following four aspects need to be improved: adjusting spectral bands to meet the needs of more plants, improving luminous intensity, quantum efficiency (QE) and thermal stability. Based on this background, many measures have been adopted to ameliorate the luminescent properties of LMT:$Mn^{4+}$: (Ⅰ) choosing applicable flux. Liao et al reported that LiCl could improve the thermal stability and regulate the morphology of LMT:$Mn^{4+}$ [25]; (Ⅱ) adopting energy transfer strategy. Lin and colleagues found that co-doping with $Bi^{3+}$ can improve the thermal stability and IQE of LMT:$Mn^{4+}$ [20]. Despite these measures have been shown to significantly improve the photoluminescence performance of LMT:$Mn^{4+}$, the strategies about spectral modification were not reported.

In general, compared with $Eu^{2+}$, $Ce^{3+}$ and $Mn^{2+}$, the emission spectrum of $Mn^{4+}$ is difficult to be adjusted [26,27]. This is because when $^2E$ energy level is the lowest excited state energy level, $^2E \rightarrow {}^4A_2$ belongs to the spin forbidden transition, which is manifested as line spectral emission. The peak value is usually around 690-710 nm for oxides and 630 nm for fluorides, and the transition is little affected by the crystal field. [18,26]. However, in some particular lattice structure, the emission of $Mn^{4+}$ can be changed by modulating the local crystal field strengthen of luminescence center. Based on this, some successful cases have been reported. For example, Zhou et al reported that a 3.6 nm red shift of emission spectra was be implemented by introducing the $Ge^{4+}$-$Li^{+}$ to replace $Al^{3+}$-$Ca^{2+}$ ion pair in $Ca_{14}Ga_{10}Zn_6O_{35}:Mn^{4+}$ ($CGZO:Mn^{4+}$) phosphor. Meanwhile, the emission intensity, thermal stability and QE of $Ca_{14}Ga_{10}Zn_6O_{35}:Mn^{4+}$ were also significantly enhanced [28]. A red-shift was announced by replacing $Ge^{4+}$ with $Ti^{4+}$ ion in $Mg_{14}Ge_5O_{24}:Mn^{4+}$ phosphor [29]; Similar tunable luminescence performances are also found in $(Ba_{1-x}Sr_x)_2YSbO_6:Mn^{4+}$ phosphor due to the substitution of $Sr^{2+}$ to $Ba^{2+}$ [30]. Take inspiration from these literatures, cation substitution is a promising strategy to change the structure of the host lattice and further optimize the spectral range, thermal stability, luminous intensity and QE of phosphors. Therefore, we tried to substitute $La^{3+}$ with $Y^{3+}$ in $LMT:Mn^{4+}$ phosphor to understand the effect of the change in local structure on the photoluminescence properties of this phosphor during this process.

In this work, a novel $Mn^{4+}$-doped $La_{2-x}Y_xMgTiO_6$ red phosphor with tunable emission properties, great improved luminescent intensity, thermal stability and QE

are discovered. The crystal structure, luminescence performance, QE and thermal stability of the samples were researched by combining experimental and computational methods, including Rietveld refinement, electron microscopy, spectrum and decay time measurement. Moreover, the LED devices, which combine as-prepared phosphor with the blue chips, show bright blue and red emission which match with the plant absorption spectrum well, indicating that these materials are promising candidates in indoor plant lighting.

## 2. Experimental section

### 2.1. Samples synthesis and pc-LEDs fabrication

A range of phosphors $La_{2-x}Y_xMgTiO_6$:0.002$Mn^{4+}$ (x = 0-2) were prepared through high-temperature solid-state method. Proper amounts of $Y_2O_3$ (99.999%, Aladdin), $La_2O_3$ (99.999%, Aladdin), MgO (99%, Aladdin), $TiO_2$ (99%, Aladdin), $H_3BO_3$ (99.5%, Aladdin) and $MnCO_3$ (99.999%, Aladdin) as starting materials. According to the target compounds, the materials were weighed. Particularly, excess MgO and 2 wt%$H_3BO_3$ are added to ensure the purity of products and promote the decomposition of carbonate. Besides, a moderate amount of alcohol was also employed to blend these powders more fully. After that, the mixtures were ground adequately for 30 min, then pre-fired at 1000 °C for 8h at tube furnace. These precursors were reground for 20 min when the temperature of hearth is low enough. After that, these samples were sent in the same tube furnace and continued to sinter at 1350 °C for 24 h with a heating rate of 5 °C/min in the whole process.

The pc-LED devices were manufactured by combining as-prepared red

$La_2MgTiO_6$:0.002$Mn^{4+}$, $Y_2MgTiO_6$:0.002$Mn^{4+}$ phosphor and 460 nm blue chips. The sample phosphor was blended uniformly with epoxy resin A and B (A:B=2:1) in the agate mortar and the obtained mixture was spread on a 460 nm blue chip evenly. After that, the as-fabricated devices were transferred in an oven to solidify epoxy resin completely at 120℃ for 12 h. At last, all devices cooled down to room temperature naturally and kept in the box for characterization farther.

**2.2. Sample characterization**

Powder X-ray diffraction (XRD) patterns were measured range from 10° to 80° by a diffractometer (D/SHIMADZU-6000, Japan) with Cu-Kα radiation source (λ = 1.5406 Å). The scanning rate and operating conditions was set at 6°/min and 40 kV, 40 mA. Fine structure data including lattice parameters were recorded in a step-scanning mode obtaining by a D8 Advance diffractometer (Bruker Corporation, Germany). The step size, counting time per step and measured range was set at 0.02° , 5 s and 5° to 120°, respectively. The data of $La_2MgTiO_6$ (JCPDS No. 70-4252) and $Dy_2MgTiO_6$ were adopted as the incipient model. TOPAS 4.2 software was used to conduct the XRD Rietveld refinement [31]. The micromorphologies of the samples were investigated using a double-beam scanning electron microscope (FEI helios nanolab G3 UC, USA). F-4700 fluorescence spectrophotometer (Hitachi, Japan) equip with a 150W Xe lamp was used to obtain the PL and PLE spectra. Thermal stability was collected by a heat controller (Orient KOJI, China) in combination with F-4700 spectrophotometer. U-3310 spectrophotometer (Hitachi, Japan) was used to test the UV–vis absorption spectra. The decay times were examined by FLS920 spectrometer

(Edinburgh, UK), equipped with a Xe900 lamp. QE-2100 testing system (Otsuka, Japan) was used to collect the quantum efficiency. ATA-500 measurement system (Everfine, China) was used to test the electroluminescence (EL) spectrum of LED devices.

## 3. Results and discussion

### 3.1. Structural characterization and Micromorphologies

For the samples with $Y^{3+}$ incorporation, the XRD Rietveld refinements of $La_{2-x}Y_xMgTiO_6:Mn^{4+}$ phosphors are conducted and displayed in Fig. 1a-f. We used the data of $Dy_2MgTiO_6$ with alike structure as the incipient model, because the information of $Y_2MgTiO_6$ was lacking in the inorganic crystal information database (ICSD) [21, 22]. It could be found that most diffraction peaks, except several small impurity $SiO_2$ (usually appears after grinding), MgO and $LaTiO_3$ peaks, are indexed to the monoclinic cell ($P2_1/n$) with arguments verge on $Y_2MgTiO_6$. Although it is difficult to obtain a pure phase in the prepared sample, $Mn^{4+}$ doping in impurities had no photoluminescence emission. Therefore, a small amount of impurity phase does not affect the luminescence of the main phase. The refined parameters are collected and listed in Table 1. It could be observed that all the fraction factors ($R_{wp}$, $R_p$, $R_B$ and $\chi^2$) converged in reasonable ranges, implying that these refinements are reliable. Other refined parameters, including coordinates of atoms and main bond lengths, are listed in Supporting Information Table S1 and S2. In consideration of $r(La^{3+}) > r(Y^{3+})$, the diffraction peaks of $La_{2-x}Y_xMgTiO_6:Mn^{4+}$ shift toward larger angles as x goes up, implying a lattice shrinkage ( Fig. 1g, Fig. S1 and S2). Interestingly, when $x \leq 0.4$, the

diffraction peaks only move to a higher angle, while $x \geq 0.8$, a distinct phenomenon of peaks splitting and shift can be observed. According to the refinement results, the substitutions of $Y^{3+}$ ions for $La^{3+}$ lead to the cell volume ($V$) and lattice constants successive decrease, corresponding to the fact of $r(La^{3+}) > r(Y^{3+})$ (Fig. 1h). These results illustrate that $La^{3+}$ sites are explicitly occupied by the $Y^{3+}$ ions to form solid solutions. Furthermore, which will induce variation of local structural, and affect photoluminescence properties.

Based on the Rietveld refinement information, Fig. 1i displays the crystal structure of the monoclinic $La_{2-x}Y_xMgTiO_6$. They all belong to $A_2BB'O_6$ double perovskite structure with $P2_1/n$ space group. The $Ti^{4+}$ and $Mg^{2+}$ ions separately coordinated with six oxygen atoms to form the twisted and tilted $[TiO_6]$ and $[MgO_6]$ octahedron. They are cross-linked each other by sharing $O^{2-}$ ion in the corner, alternative arranged in two alternating face center cubic sublattices. Besides, the $La^{3+}/Y^{3+}$ ions are occupied in the vacancies between octahedrons. The corresponding $[LaO_{12}]$ polyhedron would shrink and further affect the nearby octahedral environment when the substitutions of $Y^{3+}$ for $La^{3+}$. From the effective ionic radius viewpoint, the dopant $Mn^{4+}$ (CN = 6, r = 0.53 Å) are more similar to the $Ti^{4+}$ (CN = 6, r = 0.60 Å). Moreover, the formation energy of Mn-Ti substitution is smaller than that of Mn-Mg, according to the research of Zhou et al [32]. Thus, these conditions make it reasonable to believe that $Mn^{4+}$ preferentially replaces the crystallographic sites of $Ti^{4+}$ in $La_{2-x}Y_xMgTiO_6$.

The SEM images of sample phosphor were shown in Fig. 2 and Fig. S3. Like

most phosphors synthesized by high-temperature solid-state reactions, these particles show irregular shapes with constituted by agglomerated crystals. The average diameter of particles was estimated in the range of 5-10 μm, which is in agreement with the previous literatures [20,22]. Furthermore, the EDS mapping of a single particle indicates a uniform distribution of La, Y, Mg, Ti and O across the particle. Particularly, the above results analysis was similar to the stoichiometric contents of the target except that the proportion of Mg is a little high, which could be attributed to the addition of additional MgO during the preparation process. These results indicate that the ideal phosphors $La_{2-x}Y_xMgTiO_6:Mn^{4+}$ were successfully synthesized by solid-solution methods.

### 3.2. Luminescence performance of $La_{2-x}Y_xMgTiO_6:Mn^{4+}$ phosphors

Fig. 3a-b records the PLE and PL spectra of $La_2MgTiO_6:Mn^{4+}$ and $Y_2MgTiO_6:Mn^{4+}$ phosphors at room temperature. Two typical excitation bands are observed by monitoring at optimal emission wavelength. These excitation spectra could be well decomposed into four sub-bands by Gaussian fitting, and are assigned to $Mn^{4+} \rightarrow O^{2-}$ charge transfer (CT) transition, spin-allowed $^4A_2 \rightarrow {}^4T_1$, spin-forbidden $^4A_2 \rightarrow {}^2T_2$ and spin-allowed $^4A_2 \rightarrow {}^4T_2$ transitions of $Mn^{4+}$, respectively [20,21,28]. In addition, some peak positions are found to be different between $La_2MgTiO_6:Mn^{4+}$ and $Y_2MgTiO_6:Mn^{4+}$, reflecting that $Mn^{4+}$ is in different crystal field environment. To understand this in more detail, a series of $La_{2-x}Y_xMgTiO_6:Mn^{4+}$ phosphors are prepared and measured. Fig. 3c shows the UV–vis absorption spectra of $La_{2-x}Y_xMgTiO_6:Mn^{4+}$ (x = 0, 0.4, 0.8, 1.2, 1.6, 2)

phosphors. Three correlative absorption bands ranging from 200 to 330 nm, 330 to 420 nm and 420 to 600 nm are observed for all samples, which could be attributed to host absorption, $Mn^{4+} \rightarrow O^{2-}$ charge transfer (CT) transition, the $^4A_2 \rightarrow {}^4T_1$, $^4A_2 \rightarrow {}^2T_1$ and $^4A_2 \rightarrow {}^4T_2$ transition of $Mn^{4+}$, respectively [21]. This result is well-consistent to the PLE spectra. In order to obtain more information about band structures, the optical band gaps are calculated according to the following equation [5]:

$$(\alpha hv)^n = A(hv - E_g) \quad (1)$$

where $\alpha$, $hv$ and $A$ represent the absorption coefficient, the photon energy and constant, respectively. $E_g$ is the optical band gap value. According to previous report, the value of $n$ is 1/2 since the band structures of $La_2MgTiO_6$ and $Y_2MgTiO_6$ compound are indirect [20, 21]. The band gap values for the $La_{2-x}Y_xMgTiO_6:Mn^{4+}$ (x = 0, 0.4, 0.8, 1.2, 1.6, 2) are calculated to be 3.125, 3.024, 2.915, 3.061, 3.162, 3.509 eV, respectively (see Fig. 3d). These results imply that the $La_{2-x}Y_xMgTiO_6$ matrix is a superior carrier for accommodating $Mn^{4+}$ ions as inorganic luminescence materials.

As displayed in Fig. 4a, the shape of the excitation spectrum is similar and the intensity increases with the addition of $Y^{3+}$. The emission spectra of $La_{2-x}Y_xMgTiO_6:Mn^{4+}$ phosphors upon the excitation of 350 nm are shown in Fig. 4b. Introducing a certain amount of $Y^{3+}$ could effectively improve the luminous intensity of $La_2MgTiO_6:Mn^{4+}$ phosphor, with the greatest improvement of emission intensity reached up to 201.8%. In addition, the emission spectra gradually blue-shift with a wavelength interval of 11 nm during this process, as is shown in Fig. 4c. Moreover, the change in peak shape is also particularly noticeable. Firstly, the number of

emission peaks gradually decreased from four (x = 0) to one (x = 1.2), and then increased to three (x = 2). Secondly, the strongest emission peak for $La_{2-x}Y_xMgTiO_6:Mn^{4+}$ show a blue-shift until x = 0.8 (692.6 nm), which is shorter than the emission peak of $La_2MgTiO^6:Mn^{4+}$ (710.8 nm), and then, the strongest emission peak shifted toward longer wavelengths at higher x values (see Fig. S4). The more information about luminescence spectra are listed in Table S3. It is well-known that the spectral properties of $Mn^{4+}$ ions are nearly related to the surrounding environment of octahedron. In order to further explain the blue shift observed above, the crystal splitting field energy ($D_q$) and Racah parameters ($B$, $C$) were calculated according to following formulas [33, 34]:

$$D_q = \frac{E(4_{A_{2g}} \rightarrow 4_{T_{2g}})}{10} \quad (2)$$

where the energy gap between $^4A_2 \rightarrow {}^4T_2$ transition could be ascertained by the position of peaks. In addition, the value of $B$ could be calculated on the basis of the energy difference between $^4A_2 \rightarrow {}^4T_2$ and $^4A_2 \rightarrow {}^4T_1$ transitions [33, 34]:

$$\frac{D_q}{B} = \frac{15(\alpha-8)}{(\alpha^2-10\alpha)} \quad (3)$$

where $\alpha$ is expressed as [33, 34]:

$$\alpha = \frac{E\left(4_{A_{2g}} \rightarrow 4_{T_{1g}}\right) - E\left(4_{A_{2g}} \rightarrow 4_{T_{2g}}\right)}{D_q} \quad (4)$$

By estimating the peak energy of $^2E \rightarrow {}^4A_2$ transition, the values of parameters $C$ could be calculated as follow [33, 34]:

$$\frac{E\left(2_{E_g} \rightarrow 4_{A_{2g}}\right)}{B} = \frac{3.05C}{B} - \frac{1.8B}{D_q} + 7.9 \quad (5)$$

Thus, according to the equations (2) - (5), the values of $D_q$, $B$, $C$ and $D_q/B$ of $La_{2-x}Y_xMgTiO_6:Mn^{4+}$ phosphors could be calculated and the related data were shown

in Table 2. Tanabe-sugano (T-S) energy level diagram is a common method to explain the luminescence mechanism of $Mn^{4+}$ doped phosphors, which is presented in Fig. 4d. It is worth noting that the most energy levels are affected by the crystal field strength except $^2E$ and $^2T_1$ energy levels. Besides, the interactions between $^4T_1$, $^4T_2$ and $^4A_2$ energy level are spin-allowed transitions as $\Delta S = 0$. It can conclude that the $Mn^{4+}$ ions are exposed to a strong crystal field in the $La_{2-x}Y_xMgTiO_6$ host since the $D_q/B$ value exceeds 2.2. In addition, it should be pointed out that the crystal field splitting gradually increased as the proportion of $Y^{3+}$ increases, which would cause the ascended $^2E$ level and further result in the blue shift in emission spectrum of $La_{2-x}Y_xMgTiO_6:Mn^{4+}$ phosphors. However, this blue shift is small (around 11 nm) due to the $^2E$ and $^4A_2$ energy levels of $Mn^{4+}$ are almost parallel. Fig. 4e displays the contrastive photos and CIE chromaticity coordinates diagram of samples under daylight and 365 nm UV lamp, implies that these are fine red glowing materials.

### 3.3. Temperature-dependent luminescence and decay lifetimes of $La_{2-x}Y_xMgTiO_6:Mn^{4+}$ phosphors

It is necessary to measure the luminous performance of phosphor at high temperature, because the temperature of LED devices will reach about 150 °C when working. Thus, the temperature-dependent luminescence of $La_{2-x}Y_xMgTiO_6:Mn^{4+}$ phosphors are measured and collected, as shown in Fig. 5a-e and Fig. S5. Clearly, the emission intensity decreases as the temperature increases in these samples. In addition, these peaks shape and position remain almost unchanged at different temperature. Interestingly, the anti-Stokes emission intensity (620−680 nm) of

$La_{2-x}Y_xMgTiO_6:Mn^{4+}$ (x = 1.6-2) increases first and then decreases as the temperature increases. The reason is that the anti-Stokes sideband (upper levels) can be thermally depopulated from the Stokes sideband (lower levels) to reach thermal equilibrium when the temperature increases [21]. Furthermore, Fig. 5f shows the variation of the peak intensities of above samples with the temperature. In general, at 150 °C, the thermal stability of $La_{2-x}Y_xMgTiO_6:Mn^{4+}$ decreases from 56.9% of $La_2MgTiO_6:Mn^{4+}$ to 50.3% then increase to 79% of $Y_2MgTiO_6:Mn^{4+}$ with the increase of *x* from 0 to 2, which indicating the modulation of $Y^{3+}$ in crystal structure can improve the thermal stability of $La_{2-x}Y_xMgTiO_6:Mn^{4+}$. The above improvement and variation of thermal stability are possibly attributed to the band gap. The decrease of the band gap will easily decrease the difference in energy between the lowest $^4A_2$ state and the conduction band, and cause thermal-associated ionization, which is the so-call photoionization process [35]. According to the previous results, the trend of band gap values is roughly consistent with the regular pattern of thermal stability. Therefore, the band gap seems to play a major role in causing this variation. Normally, as the band gap decreases, the luminous lifetime shortens due to the extra contribution of non-radiation in decay process [36]. On the basis of this corollary, lifetimes expectancy should follow a similar pattern. Therefore, the associated decay lifetimes are measured and discussed.

Fig. 6a-b presents the decay curves of $La_{2-x}Y_xMgTiO_6:Mn^{4+}$ excited at 350 nm and monitored at their optimal emission wavelengths. All of these curves could be well-fitted via single-exponential decay model, its expressed as follow [37]:

$$I_t = I_0 + Aexp\left(\frac{-t}{\tau}\right) \quad (6)$$

where $I_t$ and $I_0$ are the luminescence intensity at time t and time 0, $A$ refer to a constant and $\tau$ stand for the exponential component of the decay time. The calculated lifetime of $La_{2-x}Y_xMgTiO_6:Mn^{4+}$ is a single exponential verified that the single $Mn^{4+}$ emission center at $Ti^{4+}$ site, which is in consistent with the analysis of the crystal structure. Notably, the PL lifetime decreased at first with the addition of $Y^{3+}$ and then increased with the continuous addition of $Y^{3+}$, which is along with the result as predicted in the previous discussion. To better explain the decay lifetimes mechanism of above samples, the local structures diagram of solid solution as shown in Fig. 6c. During the substitution process, the overall contraction and the local expansion of the cell have a competitive relationship, affecting the local [$Mg/TiO_6$] octahedron. When the small amount of $Y^{3+}$ was added, the surrounding [$Mg/TiO_6$] octahedron would expand due to the relatively smaller ionic radius of $Y^{3+}$. If $Mn^{4+}$ occupied $Ti^{4+}$ of these inflated octahedrons, the Mn-O bond length is bound to be longer. Longer Mn-O bond length implies that its $Dq$ is smaller, which would lead to the lowered $^4T_2$ energy level (blue line) because $10Dq$ and energy level of $Mn^{4+}$ ($^4T_2$) are positively correlated. Eventually which increase the non-radiation transition, resulting in the attenuated decay lifetimes in $La_{2-x}Y_xMgTiO_6:Mn^{4+}$. As mentioned in the refinement results above, doping $Y^{3+}$ causes the crystal lattice to shrink. Therefore, the overall shrinkage would be more advantageous when x continued to increase, resulting in shorter Mn-O bond length and higher $^4T_2$ energy level (red line). Therefore, the decay lifetime of as-prepared phosphors began to increase with the continuous addition of $Y^{3+}$.

QE is a key parameter in the practical application of phosphors. Keeping this in mind, the IQE and EQE of LMT:$Mn^{4+}$ are measured to be 32.5% and 22.2%, respectively, which are similar to Lin's report [20]. Obviously, these values enhanced to 55.5% and 42.5% after $Y^{3+}$ doped. The as-prepared samples show superior IQE compared with other reported $Mn^{4+}$ activated double perovskite-type phosphors, such as $SrLaMgSbO_6:Mn^{4+}$ (35%), $Ca_2GdTaO_6:Mn^{4+}$ (33%), indicates that these materials have wider applications [38-40].

### 3.4. Application of $La_{2-x}Y_xMgTiO_6:Mn^{4+}$ in agriculture lighting

According to the above discussion, $La_{2-x}Y_xMgTiO_6:Mn^{4+}$ phosphors have red emission and excellent thermal stability performance. Therefore, it is very significant to investigate their potential application in agriculture lighting. Based on this case, we chose $La_2MgTiO_6:Mn^{4+}$ and $Y_2MgTiO_6:Mn^{4+}$ phosphors as examples to fabricate the LEDs. The devices were obtained by the combination of blue chips with above phosphors. Fig. 7a-b shows the corresponding EL spectra of $La_2MgTiO_6:Mn^{4+}$ and $Y_2MgTiO_6:Mn^{4+}$ phosphor LED devices, respectively. The spectra imply that the deep-red-light component increases obviously when the weight ratio of phosphor to resin increases, as shown the insets in Fig. 7a-b, the light emitted by LED devices changed from blue to purple. The CIE chromaticity coordinates of these devices are shown in Fig. 7c. As to $La_2MgTiO_6:Mn^{4+}$, it changed from (0.1438, 0.0404) of LED1 to (0.1829, 0.0846) of LED4. Similarly, for $Y_2MgTiO_6:Mn^{4+}$, it transfers from (0.1478, 0.0405) of LED5 to (0.1973, 0.0693) of LED8. All this reveals an important phenomenon that the increased red component. It is well known that plants will grow

faster if the light meets the requirements of plant absorption. Thus, the EL spectra of LED2 and LED6 are detailed compared with the absorption band of plant pigments, as shown in Fig. 7d. It can be clearly seen that the EL spectra of as-prepared LEDs could fit the absorption spectra of Chlorophyll B and $P_{FR}$ well. In briefly, by choosing different kinds of $La_{2-x}Y_xMgTiO_6:Mn^{4+}$ phosphors or adjusting the dosage of phosphors could meet the demands of different plants for light at various growth stages. In order to further investigate the stability of as-fabricated LEDs under different driven current, the EL spectra of LED4 and LED8 were measured under different driven current from 20 to 200 mA (see Fig. 7e). It can be clearly seen that the CIE chromaticity coordinates changed from (0.1829, 0.0846) to (0.1602, 0.0861) of LED4 and (0.1973, 0.0693) to (0.1928, 0.0771) of LED8. The slight change of CIE chromaticity coordinates testifying that as-prepared devices are less affected by driven current. However, LED fabricated from $Y_2MgTiO_6:Mn^{4+}$ has better stability at high input power compared with $La_2MgTiO_6:Mn^{4+}$. All in all, the LED devices display the excellent EL properties, and their EL spectrum matches well with the absorption band of plant pigment, indicates the $La_{2-x}Y_xMgTiO_6:Mn^{4+}$ phosphors have a potential value in agriculture lighting.

## 4. Conclusions

In this work, the new double perovskite type solid solution phosphors of $La_{2-x}Y_xMgTiO_6:0.002Mn^{4+}$ with controllable luminescence performance were designed and prepared. The analysis of XRD refinement shows that the doping of $Y^{3+}$ in $La_2MgTiO_6:Mn^{4+}$ will cause the shrinkage of the crystal lattice, resulting the peaks

shift toward a higher angle. The as-prepared phosphors present bright red emission through typical $^2E \rightarrow {}^4A_2$ transition of $Mn^{4+}$. Its emission band shifts about 11 nm with the continuous addition of $Y^{3+}$ from $La_2MgTiO_6:Mn^{4+}$ to $Y_2MgTiO_6:Mn^{4+}$, and such blue shift phenomenon could be attributed to the crystal field splitting. In addition, the IQE and EQE of $La_{2-x}Y_xMgTiO_6:Mn^{4+}$ improved from 32.5% and 22.2% to 55.5% and 42.5% after a certain amount of $Y^{3+}$ doped. More importantly, the thermal stability is prominently enhanced after entire substitution of $La^{3+}$ by $Y^{3+}$ with increasing 26% at 150℃. The as-fabricated pc-LEDs based on $La_{2-x}Y_xMgTiO_6:Mn^{4+}$ phosphors have been applied in plant growth LED lighting and demonstrated potential applications. The spectroscopic properties of the $Mn^{4+}$-doped $La_{2-x}Y_xMgTiO_6$ are an example of advances in controlled photoluminescence tuning.

**Acknowledgements**

The authors would like to gratefully acknowledge funds from the National Natural Science Foundation of China (Grant No. 21706060, 51703061, 51974123), the Hunan Graduate Research and Innovation Project (Grant No. CX2018B396), the Hunan provincial Engineering Technology Research Center for Optical Agriculture (Grant No. 2018TP2003), the Scientific Research Fund of Hunan Provincial Education Department (15K058, 19C0903) and the Natural Sciences Foundation of Hunan agricultural university, China (Grant No. 19QN11).

**Appendix A. Supplementary data**

Supplementary data to this article can be found online at https://www.sciencedirect.com/

## References


[1] Z. Zhou, M. Xia, Y. Zhong, S.J. Gai, S.X. Huang, Y. Tian, X.Y. Lu, N. Zhou, $Dy^{3+}$@$Mn^{4+}$co-doped $Ca_{14}Ga_{10-m}Al_mZn_6O_{35}$ far-red emitting phosphors with high brightness and improved luminescence and energy transfer properties for plant growth LED lights, J. Mater. Chem. C 5 (2017) 8201-8210.

[2] J. Liang, L.L. Sun, B. Devakumar, S.Y. Wang, Q. Sun, H. Guo, B. Li, X.Y. Huang, Novel $Mn^{4+}$-activated $LiLaMgWO_6$ far-red emitting phosphors: high photoluminescence efficiency, good thermal stability, and potential applications in plant cultivation LEDs, RSC Adv. 8 (2018) 27144-27151.

[3] Q. Sun, S.Y. Wang, B. Devakumar, L.L. Sun, J. Liang, X.Y. Huang, $Mn^{4+}$-activated $BaLaMgSbO_6$ double-perovskite phosphor: a novel high-efficiency far-red-emitting luminescent material for indoor plant growth lighting, RSC Adv. 9 (2019) 3303-3310.

[4] Y.J. Zheng, H.M. Zhang, H.R. Zhang, Z.G. Xia, Y.L. Liu, M.S. Molokeev, B.F. Lei, Co-substitution in $Ca_{1-x}Y_xAl_{12-x}Mg_xO_{19}$ phosphors: local structure evolution, photoluminescence tuning and application for plant growth LEDs, J. Mater. Chem. C 6 (2018) 4217-4224.

[5] Z. Zhou, Y.R. Li, M. Xia, Y. Zhong, N. Zhou, H.T. Hintzen, Improved luminescence and energy-transfer properties of $Ca_{14}Al_{10}Zn_6O_{35}$:$Ti^{4+}$, $Mn^{4+}$ deep-red-emitting phosphors with high brightness for light-emitting diode (LED) plant-growth lighting, Dalton Trans. 47 (2018) 13713-13721.

[6] Z. Zhou, Y. Zhong, M. Xia, N. Zhou, B.F. Lei, J. Wang, F.F. Wu, Tunable dual emission of $Ca_3Al_4ZnO_{10}$:$Bi^{3+}$, $Mn^{4+}$ via energy transfer for indoor plant growth lighting, J. Mater. Chem. C 6 (2018) 8914-8922.

[7] J.X. Hu, T.H. Huang, Y.P. Zhang, B. Lu, H.Q. Ye, B.J. Chen, H.P. Xia, C.Y. Ji, Enhanced deep-red emission from $Mn^{4+}$/$Mg^{2+}$ co-doped $CaGdAlO_4$ phosphors for plant cultivation, Dalton Trans. 48 (2019) 2455-2466.

[8] X.Y. Huang, H. Guo, Finding a novel highly efficient $Mn^{4+}$-activated $Ca_3La_2W_2O_{12}$ far-red emitting phosphor with excellent responsiveness to phytochrome $P_{FR}$: Towards indoor plant cultivation application, Dyes Pigm. 152

(2018) 36-42.

[9] N. Zhou, L.H. Liu, Z.P. Zhou, Y. Zhang, M.H. Li, C. Zhou, M. Xia, Z. Zhou, Engineering cation vacancies to improve the luminescence properties of $Ca_{14}Al_{10}Zn_6O_{35}$: $Mn^{4+}$ phosphors for LED plant lamp, J. Am. Ceram. Soc. 103 (2019) 1798-1808.

[10] L. Shi, Y.J. Han, Z.X. Ji, Z.W. Zhang, Highly efficient and thermally stable $CaYMgSbO_6$:$Mn^{4+}$ double perovskite red phosphor for indoor plant growth, J. Mater. Sci. – Mater. Electron. 30 (2019) 3107-3113.

[11] M. Xia, S.M. Gu, C. Zhou, L.H. Liu, Y. Zhong, Y.L. Zhang, Z. Zhou, Enhanced photoluminescence and energy transfer performance of $Y_3Al_4GaO_{12}$:$Mn^{4+}$, $Dy^{3+}$ phosphors for plant growth LED lights, RSC Adv. 9 (2019) 9244-9252.

[12] F.F. Yao, L. Wang, Y. Lv, Y.X. Zhuang, T.L. Zhou, R.J. Xie, Composition-dependent thermal degradation of red-emitting $(Ca_{1-x}Sr_x)AlSiN_3$:$Eu^{2+}$ phosphors for high color rendering white LEDs, J. Mater. Chem. C 6 (2018) 890-898.

[13] R.J. Xie, N. Hirosaki, T. Suehiro, F.F. Xu, M.J.C. Mitomo, A Simple, Efficient Synthetic Route to $Sr_2Si_5N_8$:$Eu^{2+}$-Based Red Phosphors for White Light-Emitting Diodes, Chem. Mater. 18 (2006) 5578-5583.

[14] K. Van den Eeckhout, P.F. Smet, D. Poelman, Persistent luminescence in rare-earth codoped, J. Lumin. 129 (2009) 1140-1143.

[15] J.H. Oh, H. Kang, Y.J. Eo, H.K. Park, Y.R. Do, Synthesis of narrow-band red-emitting $K_2SiF_6$:$Mn^{4+}$ phosphors for a deep red monochromatic LED and ultrahigh color quality warm-white LEDs, J. Mater. Chem. C 3 (2015) 607-615.

[16] W.M. Ming, H.L. Shi, M.H. Du, Doping $Y_2O_3$ with $Mn^{4+}$ for energy-efficient lighting, J. Mater. Chem. C 6 (2018) 4171-4176.

[17] Q. Zhou, L. Dolgov, A.M. Srivastava, L. Zhou, Z.L. Wang, J.X. Shi, M.D. Dramićanin, M.G. Brik, M.M. Wu, $Mn^{2+}$ and $Mn^{4+}$ red phosphors: synthesis, luminescence and applications in WLEDs. A review, J. Mater. Chem. C 6 (2018) 2652-2671.

[18] W. Xu, D.Q. Chen, S. Yuan, Y. Zhou, S.C. Li, Tuning excitation and emission of

$Mn^{4+}$ emitting center in $Y_3Al_5O_{12}$ by cation substitution, Chem. Eng. J. 317 (2017) 854-861.

[19] C.S. Huang, C.L. Huang, Y.C. Liu, S.K. Lin, T.S. Chan, H.W. Tu, Ab Initio-Aided Sensitizer Design for $Mn^{4+}$-Activated $Mg_2TiO_4$ as an Ultrabright Fluoride-Free Red-Emitting Phosphor, Chem. Mater. 30 (2018) 1769-1775.

[20] G.C. Xing, Y.X. Feng, M. Pan, Y. Wei, G.G. Li, P.P. Dang, S.S. Liang, M.S. Molokeev, Z.Y. Cheng, J. Lin, Photoluminescence tuning in a novel $Bi^{3+}/Mn^{4+}$ co-doped $La_2ATiO_6$:(A = Mg, Zn) double perovskite structure: phase transition and energy transfer, J. Mater. Chem. C 6 (2018) 13136-13147.

[21] P.Q. Cai, L. Qin, C. Chen, J. Wang, S. Bi, S.I. Kim, Y.L. Huang, H.J. Seo, Optical Thermometry Based on Vibration Sidebands in $Y_2MgTiO_6:Mn^{4+}$ Double Perovskite, Inorg. Chem. 57 (2018) 3073-3081.

[22] J.Q. Li, J.S. Liao, H.R. Wen, L.Y. Kong, M.H. Wang, J.L. Chen, Multiwavelength near infrared downshift and downconversion emission of $Tm^{3+}$ in double perovskite $Y_2MgTiO_6:Mn^{4+}/Tm^{3+}$ phosphors via resonance energy transfer, J. Lumin. 213 (2019) 356-363.

[23] G.C. Xing, Y.X. Feng, Z.Y. Gao, M.X. Tao, H.Q. Wang, Y. Wei, M.S. Molokeev, G.G. Li, A novel red-emitting $La_2CaHfO_6:Mn^{4+}$ phosphor based on double perovskite structure for pc-WLEDs lighting, CrystEngComm. 21 (2019) 3605-3612.

[24] J.R. Du, D. Poelman, Facile Synthesis of $Mn^{4+}$-Activated Double Perovskite Germanate Phosphors with Near-Infrared Persistent Luminescence, Nanomaterials 9 (2019) 1759-1771.

[25] M.L. Hu, C.X. Liao, L.B. Xia, W.X. You, Z.F. Li, Low temperature synthesis and photoluminescence properties of $Mn^{4+}$-doped $La_2MgTiO_6$ deep-red phosphor with a LiCl flux, J. Lumin. 211 (2019) 114-120.

[26] Z. Zhou, N. Zhou, M. Xia, M. Yokoyama, H.T. Hintzen, Research progress and application prospects of transition metal $Mn^{4+}$-activated luminescent materials, J. Mater. Chem. C 4 (2016) 9143-9161.

[27] Z.G. Xia, A. Meijerink, $Ce^{3+}$-Doped garnet phosphors: composition modification,

luminescence properties and applications, Chem. Soc. Rev. 46 (2017) 275-299.

[28] Y. Zhong, S.J. Gai, M. Xia, S.M. Gu, Y.L. Zhang, X.B. Wu, J. Wang, N. Zhou, Z. Zhou, Enhancing quantum efficiency and tuning photoluminescence properties in far-red-emitting phosphor $Ca_{14}Ga_{10}Zn_6O_{35}:Mn^{4+}$ based on chemical unit engineering, Chem. Eng. J. 374 (2019) 381-391.

[29] S.S. Liang, G.G. Li, P.P. Dang, Y. Wei, H.Z. Lian, J. Lin, Cation Substitution Induced Adjustment on Lattice Structure and Photoluminescence Properties of $Mg_{14}Ge_5O_{24}:Mn^{4+}$: Optimized Emission for w-LED and Thermometry Applications, Adv. Opt. Mater. 7 (2019) 1900093-1900108.

[30] J.S. Zhong, D.Q. Chen, S. Yuan, M.J. Liu, Y.J. Yuan, Y.W. Zhu, X.Y. Li, Z.G. Ji, Tunable Optical Properties and Enhanced Thermal Quenching of Non-Rare-Earth Double-Perovskite $(Ba_{1-x}Sr_x)_2YSbO_6:Mn^{4+}$ Red Phosphors Based on Composition Modulation, Inorg. Chem. 57 (2018) 8978-8987.

[31] Bruker AXS TOPAS V4: General profile and structure analysis software for powder diffraction data. – User's Manual. Bruker AXS, Karlsruhe, Germany. (2008).

[32] Z.W. Zhou, J.M. Zheng, R. Shi, N.M. Zhang, J.Y. Chen, R.Y. Zhang, H. Suo, E.M. Goldys, C.F. Guo, Ab Initio Site Occupancy and Far-Red Emission of $Mn^{4+}$ in Cubic-Phase $La(MgTi)_{1/2}O_3$for Plant Cultivation, ACS Appl. Mater. Interfaces 9 (2017) 6177-6185.

[33] T. Hu, H. Lin, Y. Cheng, Q.M. Huang, J. Xu, Y. Gao, J.M. Wang, Y.S. Wang, A highly-distorted octahedron with a $C_{2v}$ group symmetry inducing an ultra-intense zero phonon line in $Mn^{4+}$-activated oxyfluoride $Na_2WO_2F_4$, J. Mater. Chem. C 5 (2017) 10524-10532.

[34] T. Hu, H. Lin, F.L. Lin, Y. Gao, Y. Cheng, J. Xu, Y.S. Wang, Narrow-band red-emitting $KZnF_3:Mn^{4+}$ fluoroperovskites: insights into electronic/vibronic transition and thermal quenching behavior, J. Mater. Chem. C 6 (2018) 10845-10854.

[35] M. H. Fang, S. Mahlik, A. Lazarowska, M. Grinberg, M.S. Molokeev, H. S. Sheu, J. F. Lee, R. S. Liu, Structural Evolution and Effect of the Neighboring Cation on

the Photoluminescence of $Sr(LiAl_3)_{1-x}(SiMg_3)_xN_4:Eu^{2+}$ Phosphors, Angew. Chem. Int. Ed. 58 (2019) 7767-7772.

[36] H.X. Liao, M. Zhao, Y.Y. Zhou, M.S. Molokeev, Q.L. Liu, Q.Y. Zhang, Z.G. Xia, Polyhedron Transformation toward Stable Narrow-Band Green Phosphors for Wide-Color-Gamut Liquid Crystal Display, Adv. Funct. Mater. 29 (2019) 1901988-1901994.

[37] M. Zhao, H.X. Liao, L.X. Ning, Q.Y. Zhang, Q.L. Liu, Z.G. Xia, Next-Generation Narrow-Band Green-Emitting $RbLi(Li_3SiO_4)_2:Eu^{2+}$ Phosphor for Backlight Display Application, Adv. Mater. 30 (2018) 1802489-1802495.

[38] R.P. Cao, X.F. Ceng, J.J. Huang, X.W. Xia, S.L. Guo, J.W. Fu, A double-perovskite $Sr_2ZnWO_6:Mn^{4+}$ deep red phosphor: Synthesis and luminescence properties, Ceram. Int. 42 (2016) 16817-16821.

[39] J.S. Liao, Q. Wang, H.R. Wen, H.L. Yuan, S.J. Liu, J.X. Fu, B. Qiu, First observation of mutual energy transfer of $Mn^{4+}$-$Er^{3+}$ via different excitation in $Gd_2ZnTiO_6:Mn^{4+}/Er^{3+}$ phosphors, J. Mater. Chem. C 5 (2017) 9098-9105.

[40] L.L. Sun, J. Liang, B. Devakumar, Q. Sun, S.Y. Wang, B. Li, X.Y. Huang, Preparation, characterization, and luminescence properties of double perovskite $SrLaMgSbO_6:Mn^{4+}$ far-red emitting phosphors for indoor plant growth lighting, RSC Adv. 8 (2018) 35187-35194.

**Table 1** Crystallographic parameters obtained from XRD Rietveld refinements for $La_{2-x}Y_xMgTiO_6:Mn^{4+}$ phosphors.

| | x=0 | x=0.4 | x=0.8 | x=1.2 | x=1.6 | x=2 |
|---|---|---|---|---|---|---|
| **Space group** | $P2_1/n$ | $P2_1/n$ | $P2_1/n$ | $P2_1/n$ | $P2_1/n$ | $P2_1/n$ |
| ***a* (Å)** | 5.5579 (9) | 5.51539 (11) | 5.4702 (2) | 5.3841 (3) | 5.34094 (7) | 5.29257 (9) |
| ***b* (Å)** | 5.5587 (4) | 5.57319 (10) | 5.5856 (2) | 5.5822 (3) | 5.58944 (7) | 5.58203 (10) |
| ***c* (Å)** | 7.8591 (7) | 7.82612 (15) | 7.7868 (3) | 7.7107 (4) | 7.66703 (10) | 7.61560 (13) |
| ***V* (Å$^3$)** | 242.80 (5) | 240.562 (8) | 237.921 (16) | 231.74 (2) | 228.882 (5) | 224.988 (7) |
| ***β*** | 90.015 (8) | 90.021 (2) | 89.912 (6) | 89.898 (2) | 89.8362 (9) | 90.2435 (10) |
| $R_{wp}$ **(%)** | 9.59 | 5.26 | 5.96 | 5.18 | 3.91 | 6.05 |
| $R_p$ **(%)** | 6.96 | 4.09 | 4.41 | 3.82 | 2.90 | 4.29 |
| $R_B$ **(%)** | 5.86 | 2.26 | 1.36 | 1.50 | 0.69 | 1.10 |
| $\chi^2$ | 1.64 | 1.38 | 1.87 | 1.74 | 1.47 | 1.75 |

**Table 2** Energy states and crystal field parameters in $La_{2-x}Y_xMgTiO_6:Mn^{4+}$ phosphors.

| x | E ($4_{A_{2g}} \rightarrow 4_{T_{1g}}$) ($cm^{-1}$) | E ($4_{A_{2g}} \rightarrow 4_{T_{2g}}$) ($cm^{-1}$) | E ($2_{E_g} \rightarrow 4_{A_{2g}}$) ($cm^{-1}$) | $D_q$ | B | C | $D_q$/B |
|---|---|---|---|---|---|---|---|
| **x = 0** | 27413 | 20353 | 14084 | 2035.3 | 678.4 | 2994.1 | 3.00 |
| **x = 0.4** | 27368 | 20379 | 14084 | 2037.9 | 669.8 | 3133.0 | 3.04 |
| **x = 0.8** | 27491 | 20471 | 14450 | 2047.1 | 672.8 | 3005.8 | 3.04 |
| **x = 1.2** | 27375 | 20493 | 14409 | 2049.3 | 656.5 | 3148.0 | 3.12 |
| **x = 1.6** | 27144 | 20513 | 14347 | 2051.3 | 627.5 | 3191.9 | 3.26 |
| **x = 2** | 27346 | 20700 | 14306 | 2070 | 628.1 | 3176.2 | 3.30 |

## Figures Captions

**Fig.1.** Powder XRD Rietveld refinement patterns of $La_{2-x}Y_xMgTiO_6$: $Mn^{4+}$. (a) x=0, (b) x=0.4, (c) x=0.8, (d) x=1.2, (e) x=1.6 (f) x=2; (g) the enlarged XRD patterns of $La_{2-x}Y_xMgTiO_6$:$Mn^{4+}$ phosphors; (h) the variations of lattice parameter versus various $Y^{3+}$ doping content; (i) schematic illustration of the effect of $Y^{3+}$ doping on local crystal structures.

**Fig.2.** SEM images and elemental mapping of two characteristic particles of $La_2MgTiO_6$:$Mn^{4+}$ and $Y_2MgTiO_6$:$Mn^{4+}$ phosphor.

**Fig.3.** Multi-peaks Gaussian fitting of the excitation spectrum of (a) $La_2MgTiO_6$:$Mn^{4+}$ and (b) $Y_2MgTiO_6$:$Mn^{4+}$ phosphors; (c) the UV–vis absorption spectra of $La_{2-x}Y_xMgTiO_6$:$Mn^{4+}$ (x = 0, 0.4, 0.8, 1.2, 1.6, 2) phosphors; (d) the fitting of corresponding band gap energies.

**Fig.4.** (a) PLE and (b) PL spectra of $La_{2-x}Y_xMgTiO_6$:$Mn^{4+}$ phosphors; (c) Normalized PL spectra of $La_{2-x}Y_xMgTiO_6$:$Mn^{4+}$ phosphors; (d) the Tanabe–Sugano energy level diagram for $d^3$ electron configuration in octahedron coordination; (e) CIE chromaticity diagram of $La_{2-x}Y_xMgTiO_6$:$Mn^{4+}$ phosphors, the inset displayed the above phosphors under daylight and 365 nm UV lamp.

**Fig.5.** The temperature-dependent emission spectra of $La_{2-x}Y_xMgTiO_6$:$Mn^{4+}$ phosphors. (a) x=0, (b) x=0.4, (c) x=0.8, (d) x=1.6, (e) x=2.0; (f) the variations of normalized integrated intensities of above phosphors as functions of temperature.

**Fig.6.** (a)-(b) The decay times of $La_{2-x}Y_xMgTiO_6$:$Mn^{4+}$ phosphors upon the excitation of 350 nm and monitored at 700 nm; (c) schematic illustration of the effect of $Y^{3+}$ doping on energy level structure of $Mn^{4+}$.

**Fig.7.** (a)-(b) EL spectra of as fabricated plant growth LED1-LED8, the insets are the corresponding photographs of these LEDs; (c) CIE chromaticity diagram of LED1-LED8; the insets is the enlarged pattern; (d) the comprehensive comparison between EL spectra and the absorption curves of the plant pigments of Chlorophyll B and phytochrome $P_R$, $P_{FR}$; (e) the variation of CIE-x(y) under various driven currents.

**Fig.1**

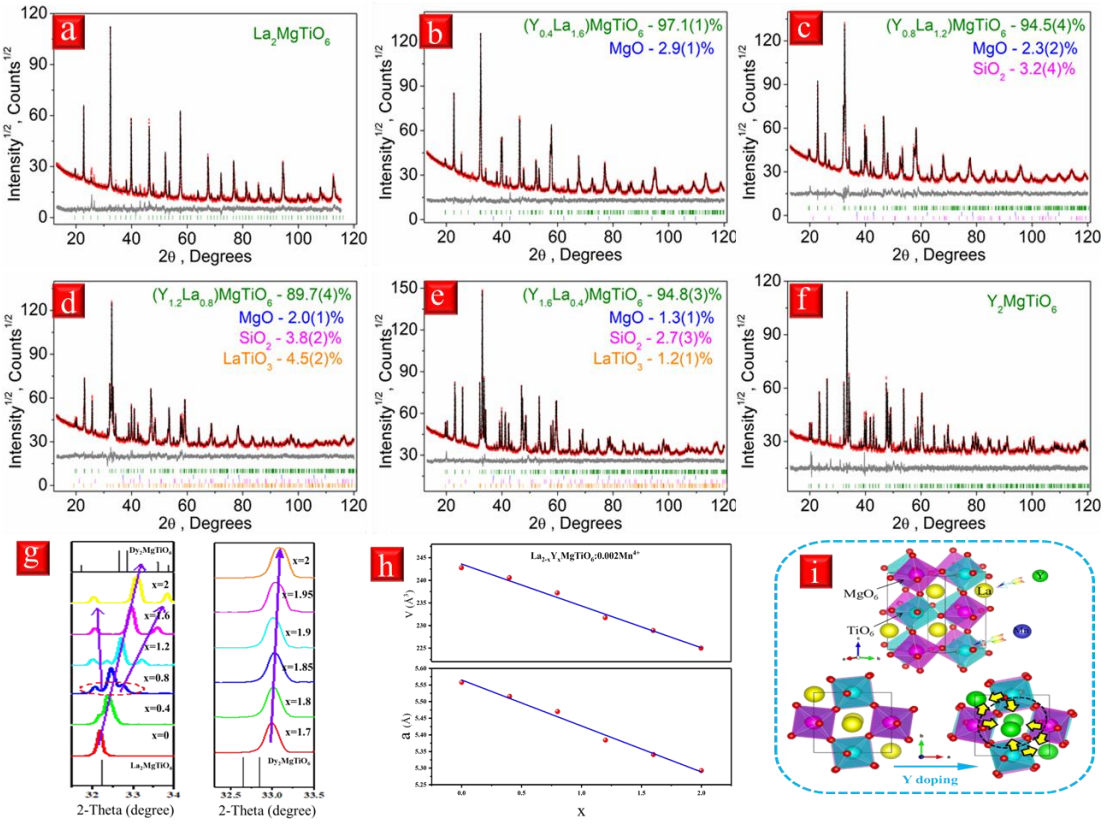
a
La2MgTiO6
b
(Y0.4La1.6)MgTiO6 - 97.1(1)%
MgO - 2.9(1)%
c
(Y0.8La1.2)MgTiO6 - 94.5(4)%
MgO - 2.3(2)%
SiO2 - 3.2(4)%
d
(Y1.2La0.8)MgTiO6 - 89.7(4)%
MgO - 2.0(1)%
SiO2 - 3.8(2)%
LaTiO3 - 4.5(2)%
e
(Y1.6La0.4)MgTiO6 - 94.8(3)%
MgO - 1.3(1)%
SiO2 - 2.7(3)%
LaTiO3 - 1.2(1)%
f
Y2MgTiO6
Intensity1/2, Counts1/2
2θ , Degrees
g
x=2
x=1.95
x=1.9
x=1.85
x=1.8
x=1.7
x=1.6
x=1.2
x=0.8
x=0.4
x=0
2-Theta (degree)
h
V (Å3)
a (Å)
x
i
MgO6
TiO6
Y doping

**Fig.2**

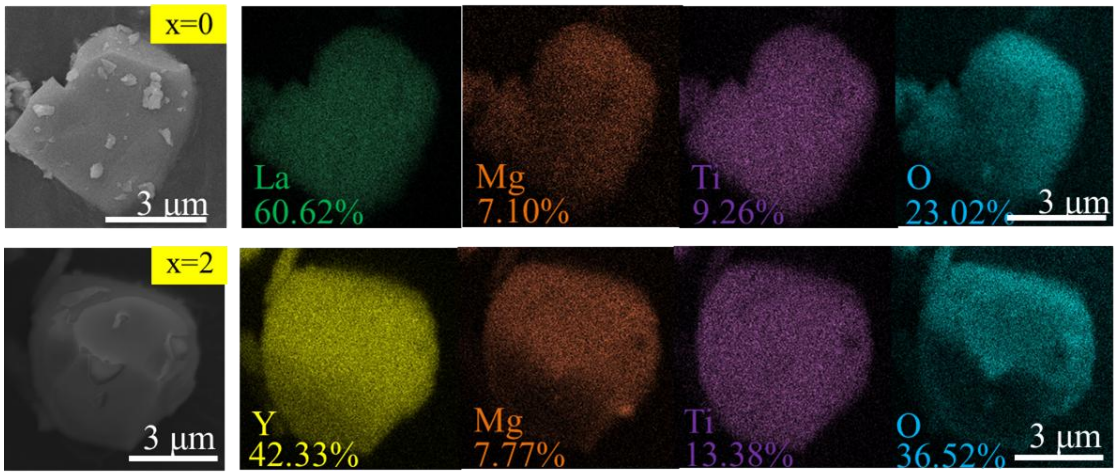
x=0
3 μm
La
60.62%
Mg
7.10%
Ti
9.26%
O
23.02%
3 μm
x=2
3 μm
Y
42.33%
Mg
7.77%
Ti
13.38%
O
36.52%
3 μm

**Fig.3**

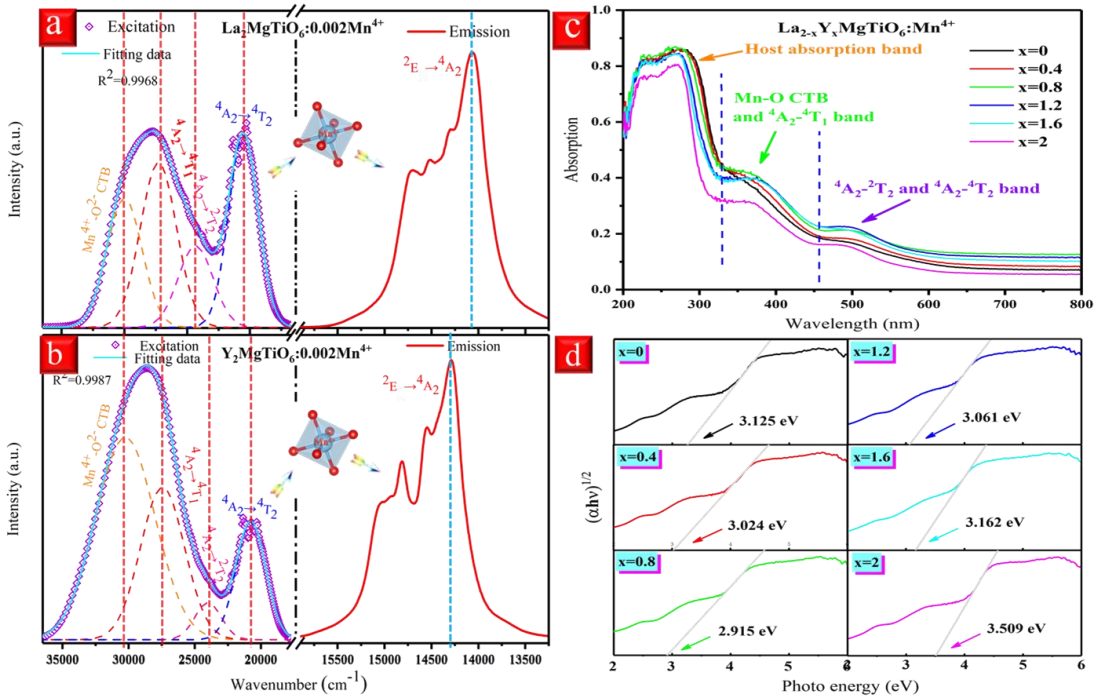
a
Excitation
Fitting data
$R^2$=0.9968
$La_2MgTiO_6$:0.002$Mn^{4+}$
Emission
$^2E \rightarrow {}^4A_2$
$^4A_2 \rightarrow {}^4T_2$
$Mn^{4+}$-$O^{2-}$ CTB
Intensity (a.u.)
b
Excitation
Fitting data
$R^2$=0.9987
$Y_2MgTiO_6$:0.002$Mn^{4+}$
Emission
35000 30000 25000 20000 15500 15000 14500 14000 13500
Wavenumber ($cm^{-1}$)
c
$La_{2-x}Y_xMgTiO_6$:$Mn^{4+}$
Host absorption band
Mn-O CTB
and $^4A_2$-$^4T_1$ band
$^4A_2$-$^2T_2$ and $^4A_2$-$^4T_2$ band
x=0
x=0.4
x=0.8
x=1.2
x=1.6
x=2
Absorption
200 300 400 500 600 700 800
Wavelength (nm)
d
x=0
3.125 eV
x=1.2
3.061 eV
x=0.4
3.024 eV
x=1.6
3.162 eV
x=0.8
2.915 eV
x=2
3.509 eV
$(\alpha h\nu)^{1/2}$
2 3 4 5 6 3 4 5 6
Photo energy (eV)

**Fig.4**

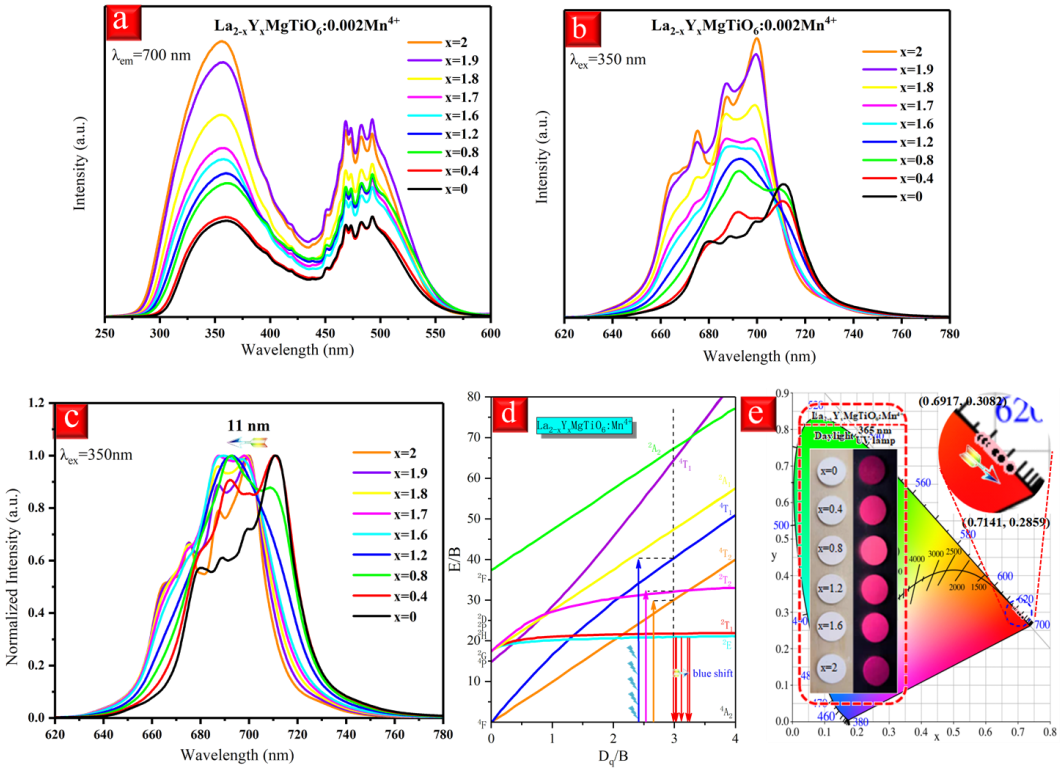
a
$La_{2-x}Y_xMgTiO_6:0.002Mn^{4+}$
$\lambda_{em}$=700 nm
x=2
x=1.9
x=1.8
x=1.7
x=1.6
x=1.2
x=0.8
x=0.4
x=0
Intensity (a.u.)
Wavelength (nm)
b
$La_{2-x}Y_xMgTiO_6:0.002Mn^{4+}$
$\lambda_{ex}$=350 nm
Intensity (a.u.)
Wavelength (nm)
c
11 nm
$\lambda_{ex}$=350nm
Normalized Intensity (a.u.)
Wavelength (nm)
d
E/B
$D_q$/B
blue shift
e
(0.6917, 0.3082)
(0.7141, 0.2859)
365 nm
Daylight
UV lamp

**Fig.5**

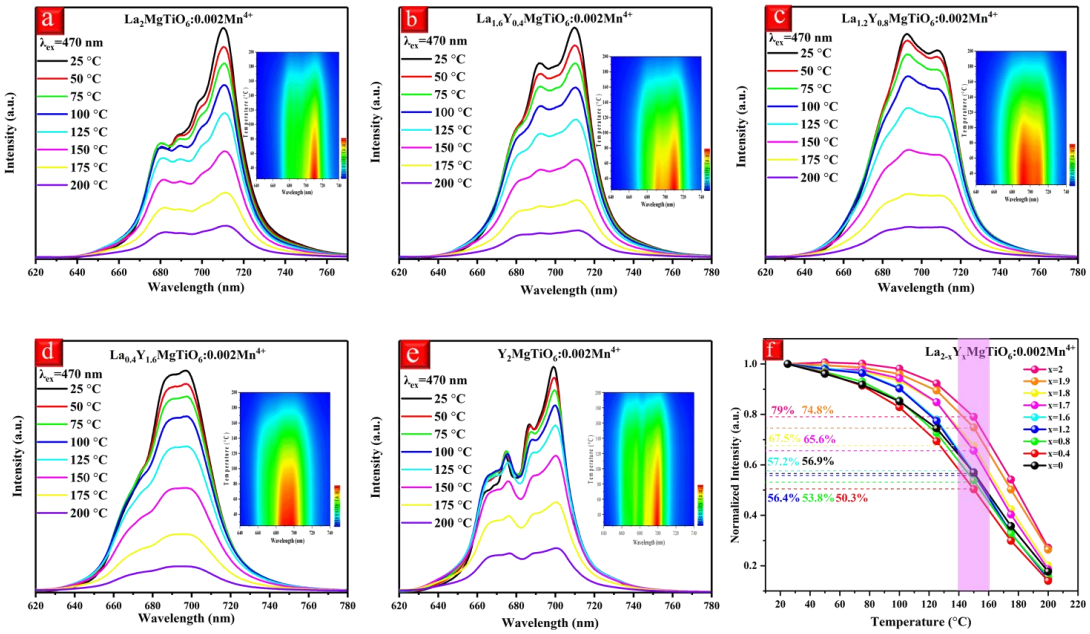
a
$La_2MgTiO_6$:0.002$Mn^{4+}$
$\lambda_{ex}$=470 nm
25 °C
50 °C
75 °C
100 °C
125 °C
150 °C
175 °C
200 °C
Intensity (a.u.)
Wavelength (nm)
b
$La_{1.6}Y_{0.4}MgTiO_6$:0.002$Mn^{4+}$
c
$La_{1.2}Y_{0.8}MgTiO_6$:0.002$Mn^{4+}$
d
$La_{0.4}Y_{1.6}MgTiO_6$:0.002$Mn^{4+}$
e
$Y_2MgTiO_6$:0.002$Mn^{4+}$
f
$La_{2-x}Y_xMgTiO_6$:0.002$Mn^{4+}$
x=2
x=1.9
x=1.8
x=1.7
x=1.6
x=1.2
x=0.8
x=0.4
x=0
79% 74.8%
67.5% 65.6%
57.2% 56.9%
56.4% 53.8% 50.3%
Normalized Intensity (a.u.)
Temperature (°C)

**Fig.6**

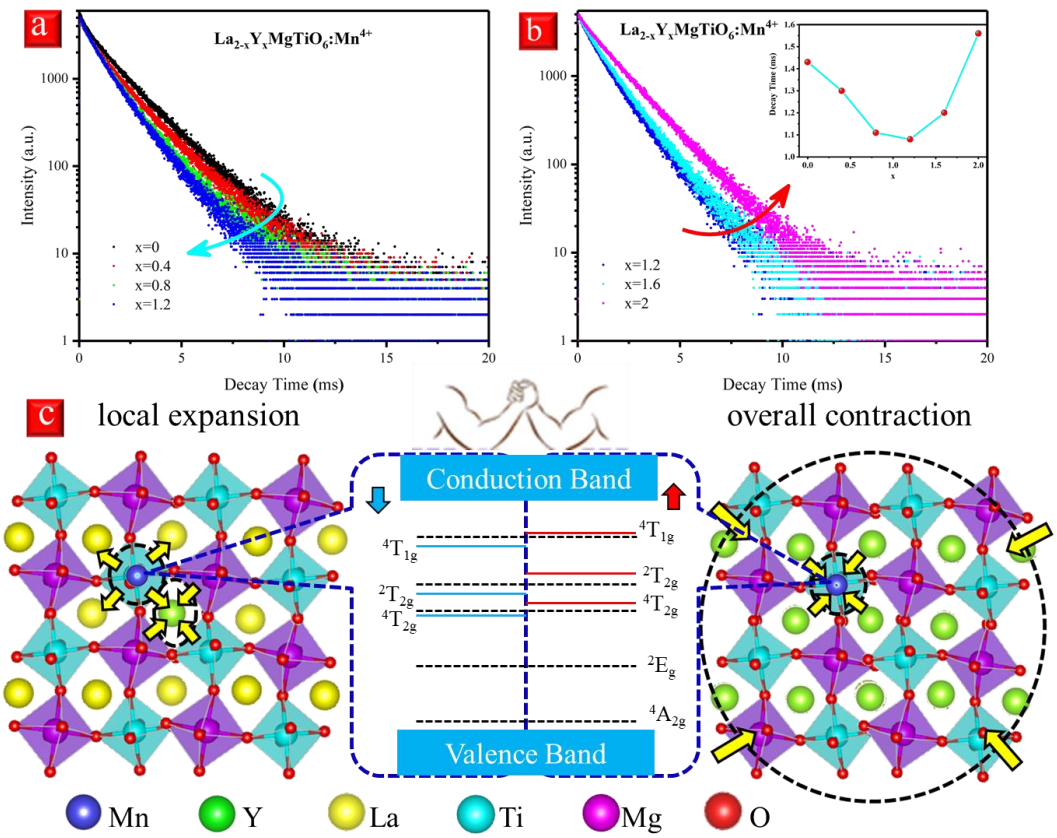
a
$La_{2-x}Y_xMgTiO_6:Mn^{4+}$
Intensity (a.u.)
Decay Time (ms)
x=0
x=0.4
x=0.8
x=1.2
b
$La_{2-x}Y_xMgTiO_6:Mn^{4+}$
Intensity (a.u.)
Decay Time (ms)
Decay Time (ms)
x
x=1.2
x=1.6
x=2
c
local expansion
overall contraction
Conduction Band
Valence Band
$^4T_{1g}$
$^2T_{2g}$
$^4T_{2g}$
$^2E_g$
$^4A_{2g}$
Mn
Y
La
Ti
Mg
O

**Fig.7**

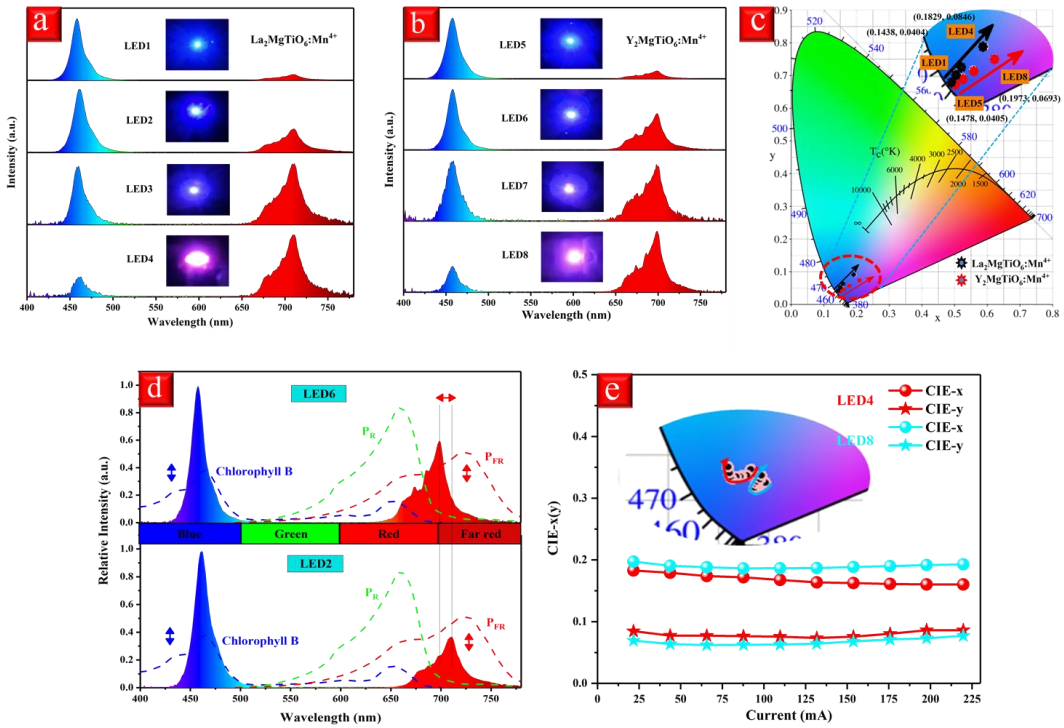
a
LED1
LED2
LED3
LED4
La2MgTiO6:Mn4+
Intensity (a.u.)
Wavelength (nm)
b
LED5
LED6
LED7
LED8
Y2MgTiO6:Mn4+
Intensity (a.u.)
Wavelength (nm)
c
(0.1829, 0.0846)
(0.1438, 0.0404)
(0.1973, 0.0693)
(0.1478, 0.0405)
LED4
LED1
LED8
LED5
Tc(°K)
La2MgTiO6:Mn4+
Y2MgTiO6:Mn4+
d
LED6
Chlorophyll B
PR
PFR
Blue
Green
Red
Far red
LED2
Chlorophyll B
Relative Intensity (a.u.)
Wavelength (nm)
e
LED4
LED8
CIE-x
CIE-y
CIE-x
CIE-y
CIE-x(y)
Current (mA)

**Supplementary Material**

**Click here to download Supplementary Material: Supporting Information.docx**

***Declaration of Interest Statement**

**Declaration of interests**

☒ The authors declare that they have no known competing financial interests or personal relationships that could have appeared to influence the work reported in this paper.

☐The authors declare the following financial interests/personal relationships which may be considered as potential competing interests: